

Article

CO Removal from Hydrogen Stream through Methanation on Ru/C Catalysts Doped with Lanthanum and Barium

Elżbieta Truskiewicz^{1,*}, Aleksandra Bielecka¹, Ewa M. Iwanek (nee Wilczkowska)¹, Milena Ojrzyńska² and Andrzej Ostrowski¹

¹ Faculty of Chemistry, Warsaw University of Technology, Noakowskiego 3, 00-664 Warsaw, Poland; abielecka59@gmail.com (A.B.); ewa.iwanek@pw.edu.pl (E.M.I.); andrzej.ostrowski@pw.edu.pl (A.O.)

² Faculty of Physics, Warsaw University of Technology, Koszykowa 75, 00-662 Warsaw, Poland; milena.ojrzyńska@pw.edu.pl

* Correspondence: elzbieta.truskiewicz@pw.edu.pl; Tel.: +48-22-2341786

Abstract: The influence of the lanthanum and barium addition on the physicochemical properties and catalytic behavior of the Ru/C catalyst for CO methanation was investigated. The catalyst was doped with La or with La plus Ba. It was found out that there are various ways the additives were applied in the study, thus changing the catalytic performance of the basic material and influencing the susceptibility of the carbon support in relation to undesired methanation. The highest catalytic activity, 23.46 (mmol CO/g_{C+Ru} × h), was achieved for the LaRu/C system, with methane selectivity exceeding 80% over the whole temperature range. Ba addition caused a significant decrease in activity. TG-MS studies revealed that both La and Ba improved the resistance of the carbon support to undesired methanation. Detailed characterization methods, employing XRPD, Raman spectroscopy, CO chemisorption, and SEM-EDX, showed that the catalytic behavior of the studied catalysts was attributed to lanthanum distribution over the Ru/C materials surface and structural changes in the carbon support affecting electron supply to the metallic active phase.

Keywords: ruthenium catalyst; carbon support; La and Ba additives; CO methanation



Citation: Truskiewicz, E.; Bielecka, A.; Iwanek, E.M.; Ojrzyńska, M.; Ostrowski, A. CO Removal from Hydrogen Stream through Methanation on Ru/C Catalysts Doped with Lanthanum and Barium. *Hydrogen* **2023**, *4*, 389–407. <https://doi.org/10.3390/hydrogen4020027>

Academic Editors: Eugenio Meloni, Marco Martino and Concetta Ruocco

Received: 16 May 2023

Revised: 9 June 2023

Accepted: 13 June 2023

Published: 20 June 2023



Copyright: © 2023 by the authors. Licensee MDPI, Basel, Switzerland. This article is an open access article distributed under the terms and conditions of the Creative Commons Attribution (CC BY) license (<https://creativecommons.org/licenses/by/4.0/>).

1. Introduction

Sustainable energy supply is critical for meeting the constantly growing energy demand [1,2], driven by population growth and technological progress. Most of this supply is currently provided by fossil fuel-based sources, significantly driving up emissions of greenhouse gases (GHG). This, in turn, contributes to undesired global climate changes [1]. Of the many available resources, hydrogen is considered as the most environmentally friendly [2,3]. Hydrogen is a clean, sustainable fuel, often called the future energy carrier [2,4,5], and it is reported to be capable of replacing/complementing the global carbon-based energy matrix [6]. According to a report published by the International Energy Agency (IEA), hydrogen and its derivatives will play an important role in the decarbonization of industrial sectors with hard-to-abate energy consumption and where alternative solutions are either unavailable or difficult to implement, such as in heavy industry, shipping, aviation, and heavy-duty transport [7,8].

In addition to its significance as an energy source, hydrogen is also an important raw material for chemical production. Out of thousands of chemical industry products, manufacturing of only 18 top products accounts for 80% of this industry's energy demand and 75% of its greenhouse gas (GHG) emissions. Energy intensity in manufacturing of those products could be greatly reduced by catalyst and related process improvements, leading to significant energy savings and decrease in carbon dioxide emissions [7]. The chemical industrial branch of hydrogen consumption is dominated by fertilizer production in the ammonia industry, oil refining, methanol synthesis, as well as iron and steel manufacturing [6]. Of these, the first three strictly involve the use of catalysts. In the case of

ammonia production, the whole process of synthetic gas preparation requires the use of many catalytic processes [3]. For the abovementioned reasons, studies concerning catalysts improvements continue to have high importance and attract interest.

There are several methods of hydrogen purification for practical purposes [3,9–12], out of those many are catalytic processes. For decades, catalytic methanation of carbon oxides has been commonly applied for hydrogen purification in ammonia plants [13] and for fuel cell purposes [14,15]. Supported nickel catalysts are commonly used in industrial methanation [16,17]. Among other metals exhibiting activity in this reaction [18], ruthenium, in particular, has been the subject of substantial interest over the years [19–21] due to its high activity [22]. Ruthenium catalysts have also been implemented in industrial practice [22,23]. The activity of ruthenium catalysts in carbon oxide methanation depends on many factors [24], such as Ru particle size [25,26], type and the specific surface area [24–28] of the support, or presence of additives [29–33]. Among various materials used as supports for ruthenium catalysts for CO methanation, carbon-derived ones are the most popular. It must be noted that different carbon supports are widely used in the industrial applications for metallic catalysts designated to operate in hydrogen-containing streams. Such important industrial processes include ammonia synthesis/decomposition, Fischer–Tropsch synthesis, and hydrogenation/dehydrogenation reactions, including CO methanation [34].

High activity of a Ru–Zr catalyst supported on carbon nanotubes in selective CO methanation was reported by Xiong [35], along with high CO hydrogenation selectivity. Good performance of Ru–ZrO₂/carbon nanotube–Ni foam composites in selective CO methanation was also described by Xiong [36]. High CO selectivity and excellent catalytic stability of these catalysts was attributed to thermal conductivity and unique microstructure of the support material [36]. The structure of carbon support material determines the Ru particle size [28], as well as its dispersion and interaction with the support. Jimenez studied this effect with the use of carbon nanofibers of different structure [37]. The authors indicated that the textural properties and amount of acidic oxygen-containing groups in the used supports are clearly dependent on the orientation of the graphitic sheets in the material and, thus, determine the active phase properties [37]. In a paper published by Kumi [38], functionalized and un-functionalized carbon spheres were used to support Ru nanoparticles for CO methanation. Both catalyst types completely converted CO within a temperature range of 240–300 °C [38]. It was revealed that the functional groups on the surface of the carbon support affected the course of reduction in the active phase, determining its dispersion and final activity [38]. The potential of partly graphitized carbons as a support for ruthenium was described in our previous works [28,39].

The general problem connected with application of carbon supports is a risk of their methanation. Interaction of hydrogen activated on the surface of the metal particles with carbon atoms of the support results in formation of methane [34]. There are two factors facilitating the intensity of this undesirable process: a high dispersion of the supported metal particles and the presence of the reactive globular carbon of disordered structure [34]. Methanation of the carrier ultimately threatens to deactivate or even destroy the catalyst. Fortunately, the addition of some modifiers can inhibit this process [34].

While the role of barium in increasing the protection of carbon support in relation to undesired methanation is clear [40–43], its potential as a promoter for CO_x methanation catalysts is rather questionable [40]. On the other hand, the promoting influence of lanthanum on the activity of catalysts for the abovementioned process was confirmed in several works. The beneficial influence of physicochemical properties, e.g., basic sites, oxygen vacancies, and oxygen mobility upon the addition of La³⁺ to the support has been described in [44–48]. Transient isothermal isotopic exchange (TIIE) experiments, involving ¹⁶O/¹⁸O, have shown that the incorporation of lanthanum into a Ce–Cu–O system improved oxygen mobility in these systems, which had a positive effect on their activity in CO oxidation [44]. In the case of methanation reactions, the positive effect of lanthanum on the catalyst activity was attributed to the increased formation of basic sites on the surface [45–47], which led to better dispersion of hydrogen [45] and stabilization of the active sites [46,47]. Quindimil [49]

reported that the considerable increase in basicity of a Ni/BETA zeolite catalyst, connected with high dispersion of nickel, was obtained upon introduction of different loadings of La_2O_3 . As a consequence, a significant increase in activity and selectivity towards CH_4 in CO_2 methanation was observed [49]. Zhang [50] reported that the presence of lanthanum modifier in a nickel phyllosilicate catalyst played a significant role in providing high nickel dispersion and excellent catalytic performance in CO_2 methanation. Wierzbicki [51] described lanthanum-doped Ni/hydrotalcite-derived catalysts for a CO_2 methanation reaction, exhibiting high activity at 300 °C, with CO_2 conversions around 36–87% and selectivity towards CH_4 above 98%. A promoting influence of La on the activity of ruthenium catalysts was described by Tada [52,53] for the Ru/ TiO_2 system. The increase in CO methanation activity upon La introduction was attributed to the increased electron density on the active phase particles, which facilitates the dissociation of the adsorbed CO. In our last work, we showed that lanthanum added to Ru/carbon systems acts as a promoter, leading to the increase in the catalytic activity in CO methanation [29]. At the same time, it facilitates the inhibition of undesired carbon support methanation, as reported in [54].

Another important physicochemical issue, which influences the activity of catalysts in CO_x methanation, is the deposition of carbon [48]. Time-on-stream tests can indicate deposit formation by a loss of activity, although other reasons for the loss of activity cannot be ruled out on the basis of these results alone. In the case of carbon-supported systems, the only way to differentiate the carbon support from the carbon deposit is to investigate the differences in the morphology of the two types of carbon, which can be determined via TEM or SEM imaging.

The question we asked ourselves was whether the promoting effect of lanthanum would be maintained in co-existence with barium in doubly doped catalysts for increased resistance to support methanation. In the literature, there are no examples of using Ba + La in one catalytic system for CO methanation. Scanty study reports concern simultaneous application of lanthanum and barium in Fischer-Tropsch synthesis catalysts. Zamani [55] observed the synergetic effect of La and Ba promoters on a nanostructured iron catalyst in that process. The recorded improvement of the catalytic performance was attributed to the modifications of H_2 and CO adsorption processes, caused by the presence of promoters [55]. However, despite some similarities between CO methanation and FTS reaction, it is difficult to transfer conclusions presented in [55] to CO methanation. The novelty of our work is the application of these two elements in one ruthenium catalytic system supported on modified carbon. Our aim was to check if barium added to LaRu/C system would have a positive effect on the carbon support stability against undesired methanation, simultaneously, without losing the recently revealed [29] promoting effect of lanthanum. In our work, we prepared a series of Ru/graphitized carbon catalysts doped with lanthanum or lanthanum and barium, introduced simultaneously, onto the Ru/C surface.

2. Materials and Methods

2.1. Catalysts Synthesis

The carbon support was obtained through high-temperature treatment of commercial RO 08 active carbon (Norit B.V. Company, Amersfoort, The Netherlands): 1900 °C, 2 h, 4 mbar argon pressure. Next, the material was washed with distilled water, dried in air at 120 °C, and used for catalyst preparation. The ruthenium precursor ($\text{RuCl}_3 \cdot 0.5\text{H}_2\text{O}$, Sigma Aldrich, St. Louis, MO, USA) was introduced onto the support surface by wet impregnation [39] from an acetone solution containing the appropriate amount of ruthenium salt to obtain 5 wt.% Ru loading. After drying, the material was reduced in flowing hydrogen and passivated according to the procedure described in [39]. In consequence, a Ru/C catalyst was obtained. The desired loading of lanthanum/lanthanum + barium was obtained by dry impregnation, as described in [39], with the use of aqueous solutions of carefully weighed portions of La nitrate or a mixture of La and Ba nitrates. The La content was the same in all La-containing samples, namely, 0.03 La/Ru molar ratio. Two samples doped with Ba were prepared with a 0.1 and 0.2 Ba/Ru molar ratio. After the introduction

of the desired amounts of nitrates, the three doped materials—LaRu/C, Ba_{0.1}LaRu/C, and Ba_{0.2}LaRu/C—were dried in air at 90 °C overnight. All catalysts were labelled with symbols that were specified in sequence: the Ba content, La symbol, Ru symbol, and carbon support, e.g., Ba_{0.1}LaRu/C. Selected samples were additionally treated in hydrogen flow (80 mL/min) for 10 h at 420 °C to simulate the changes occurring in course of catalyst activation. They were labelled as, e.g., Ba_{0.2}LaRu/C red.

2.2. Characterization Studies

The textural parameters of the carbon support and freshly prepared catalysts, specific surface area (S_{BET}), total pore volume (V_{p}), and average pore diameter (D_{p}) were evaluated by N₂ adsorption at −196 °C with the use of ASAP2020 (Micromeritics) [56]. Before analysis, the samples were degassed under vacuum for 1 h at 90 °C and, next, they were degassed for 4 h at 300 °C. The obtained results were approximated by the Brunauer-Emmett-Teller (BET) and Barrett-Joyner-Halenda (BJH) adsorption isotherm models to determine S_{BET} , V_{p} , and D_{p} . The experimental uncertainty in S_{BET} , V_{p} , and D_{p} was ±1%.

Powder X-ray diffraction experiments were performed for powdered samples, as described in [56]. A Bruker D8 Advance diffractometer, operating with Cu-K α radiation ($\lambda = 0.154$ nm) and equipped with a LYNXEYE position sensitive detector, was applied. Data were collected under standard laboratory conditions (temperature and relative humidity) in the Bragg-Brentano geometry within 2θ angle range 10°–90° with step 0.03°, as well as 10 s/step, at room temperature. The Scherrer equation [57] ($k = 0.89$) was used to calculate the average Ru crystallite sizes in selected samples.

All the samples were characterized by conventional CO chemisorption volumetric experiments, described in [39] with use of an ASAP 2020 instrument (Micromeritics). After reduction in hydrogen (80 mL/min) at 430 °C for 10 h, the sample (mass 0.2 g) was cooled to 35 °C and exposed to CO in the pressure range 50–450 mmHg.

The H₂-TPR measurements were performed in a thermogravimetric setup coupled with a mass spectrometer, according to the procedure presented in [40]. Netzsch STA 449C thermobalance equipped with a quadrupole mass spectrometer (Netzsch QMS 403C) was used for these measurements. The powdered samples (approximately 20 mg) were heated in a pure H₂:Ar = 1:1 mixture (100 mL/min) up to 600 °C at the constant rate of 10 °C/min. Next, the temperature was maintained constant at 600 °C for 2 h. The mass change, temperature, and selected m/e signals were monitored during the whole experiment. All the necessary apparatus parts were kept heated to 250 °C to avoid water condensation.

Samples were subjected to Statistical Raman Spectroscopy with Raman mapping technique. Materials were measured in powder form on a holder with Renishaw inVia Qontor confocal Raman microscope using a 532 nm, 45 W laser with an 1800 L/nm grating as the light source. A static range with a centre of 2080 cm^{−1}, 5% power of laser, with an exposure time of 5 s, as well as 200 points on each sample with 4 μm distances between measurement points, was applied.

SEM images were acquired with a Helios PFIB microscope from ThermoScientific, equipped with an integrated EDX analysis system in high vacuum mode using both an Everhart-Thornley Detector (ETD, secondary electrons) and a Circular Backscatter Detector (CBS, back-scattered electrons), with a working distance of 6–8 mm, as well as an accelerating voltage of 15 kV, at different magnifications. The EDX elemental maps were obtained using the same parameters with the Drift Correction function enabled and were analyzed with APEX software.

2.3. Catalytic Activity Studies

The catalytic activity of the prepared samples in CO hydrogenation was tested in a tubular flow-through glass reactor in a setup described in [39], in accordance with the procedure reported in the same work. A model, simplified gas mixture, containing CO + H₂, was used for catalytic tests. In short, small samples of constant Ru + C mass (0.02 g), diluted with 0.1 g quartz particles to improve mass and heat transfer, were activated in flowing H₂

(40 mL/min) at 370 °C for 17 h. After cooling to 270 °C, the gas stream was switched to CO (1 vol.%) + (99 vol.%) H₂ (total gas flow 80 mL/min) and tested for the CO methanation reaction in the temperature range of 200–270 °C under atmospheric pressure. The use of mass flow controllers ensured the precise and stable composition of the inlet gas stream. After 1 h of stabilization at each temperature, the outlet gas composition was monitored with a gas chromatograph (Trace 1310, Thermo Scientific, Waltham, MA, USA) equipped with a CO_x methanizer and a Flame Ionized Detector. The deviation of GC data was within 5% (usually less than 2%). The total conversion of carbon monoxide was calculated on the basis of its inlet–outlet mass balance. The reaction rate of CO hydrogenation, normalized to the same support + Ru mass in the sample, was calculated from the CO conversion, the inlet molar flow rate of CO, and the mass of C + Ru in each sample tested. Selectivities towards different products were calculated as the ratio of outlet amount of particular product compared to the overall amount of CO converted.

The time-on-stream test was performed for the Ba_{0.1}LaRu/C catalyst to determine how the presence of barium impacts the long-term activity of the doubly-doped system (TOS of LaRu/C can be found in our previous work [29]). After the activity measurements, the catalyst was overheated at 300 °C in the CO + H₂ (1:99 vol:vol) gas mixture (80 mL/min) at 0.1 MPa. Next, after 24 h and 96 h of time-on-stream, the activity was measured again.

3. Results

3.1. N₂ Physisorption

Table 1 summarizes the texture properties of the catalysts and carbon support obtained with N₂ adsorption measurements. They were performed for pure support and Ru/C material after ruthenium introduction and reduction. La and Ba-doped materials were characterized after La/Ba salts impregnation on the Ru/C material. Therefore, these samples contained two elements in their uncalcined forms.

Table 1. Physicochemical properties of the catalysts and carbon support; S_{BET}—specific surface area estimated based on the BET isotherm model, V_p—total pore volume estimated based on the BJH isotherm model, D_p—average pore diameter estimated based on the BJH isotherm model.

Sample Symbol	S _{BET} (m ² /g)	V _p (cm ³ /g)	D _p (nm)
C	50.72	0.0705	4.75
Ru/C	45.97	0.0669	5.23
LaRu/C	47.90	0.0683	4.95
Ba _{0.1} LaRu/C	35.79	0.0549	5.33
Ba _{0.2} LaRu/C	42.38	0.0601	5.01

Impregnation of the support with the ruthenium salt, followed by its reduction to metallic ruthenium, caused about 9% decrease in the specific surface area from 50.72 to around 46 m²/g. It is probably due to the blockage of pores of carbon with ruthenium. Consequently, the total pore volume slightly decreased, and the average pore diameter increased by 10%. Introduction of lanthanum nitrate onto the surface of Ru/C material caused a little improvement in the texture properties. A slight rebuild of surface area was observed for LaRu/C, accompanied by a small increase in pore volume and lowering of the D_p parameter. The opposite, but more expected result, was observed in the case of the doubly doped catalysts. It should be noted that the impregnation solution contained both salts simultaneously. After the deposition of La + Ba precursors onto the Ru/C material, both S_{BET} and V_p decreased because the nitrate particles blocked the pores. What is surprising, however, is that a lower S_{BET} value was observed for Ba_{0.1}LaRu/C than for Ba_{0.2}LaRu/C. Other textural parameters (Table 1) consequently revealed that the lower amount of barium in the impregnation solution interacts with lanthanum salt in a different manner, which caused worse textural properties compared to Ba_{0.2}LaRu/C.

Figure 1 shows the pore size distributions of the carbon support and four Ru/C-based catalysts. As seen in Figure 1, the studied materials had a mesoporous structure.

The pore size distribution plots exhibited, in general, bimodal forms. Two peaks were registered. First, a high and narrow signal was obtained at about 3–5 nm pore diameter for all studied materials. Its area was the largest for the support material (C) and the lowest for the Ba0.1LaRu/C sample. This effect is consistent with the textural data collected in Table 1, since the smallest pores have the most significant impact on the specific surface area. Introduction of any additional components on the support caused the decrease in this peak, and its maximum was shifted toward larger pore sizes. This is connected with the blockage of small pore entrances with deposited particles. The second broad peak was observed in a range of 30–80 nm pore diameters. The shape of that signal changed slightly with sample composition, but no significant effects were observed.

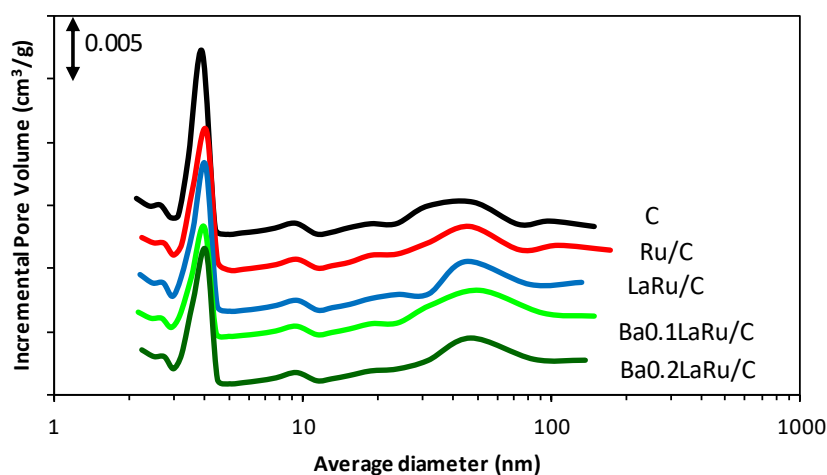


Figure 1. Pore size distributions of carbon support and ruthenium catalysts are determined by nitrogen physisorption.

3.2. CO Chemisorption

Static measurements of CO chemisorption were conducted to determine the amounts of CO adsorbed ($\mu\text{mol CO/g catalyst}$) on the surfaces of the catalysts. The ratio of CO molecules adsorbed with respect to the total metal atoms in the sample (Ru, La, Ba) were presented in Table 2. Taking the latter into calculations, the ruthenium dispersion and its average particles size were calculated for undoped Ru/C catalyst (d_{Ru}) with the use of the literature equations [58].

Table 2. CO chemisorption data of the Ru/C-based catalysts.

Catalyst	Metal Atoms (mmol/g _{cat})	CO Adsorbed ($\mu\text{mol/g}_{\text{cat}}$)	CO/Metal Atoms in the Sample (mol/mol)	d_{Ru} (nm)
Ru/C	0.495	55.1	0.111	7.1
LaRu/C	0.507	35.9	0.071	-
Ba0.1LaRu/C	0.549	18.1	0.033	-
Ba0.2LaRu/C	0.594	11.8	0.020	-

As presented in Table 2, the highest amount of adsorbed CO was obtained for unpromoted Ru/C. The average ruthenium crystallite size for this system was 7.1 nm. The former research performed in our lab revealed that both lanthanum and barium, supported on modified carbon subjected to applied experimental conditions, adsorbed low, but detectable, amounts of CO: 0.011 mmol CO/mmol La and 0.004 mmol CO/mmol Ba. Therefore, in the case of La- and La+ Ba-doped materials, the CO adsorption cannot be attributed solely to ruthenium. As a consequence, for these materials, the ruthenium dispersion and its crystallites sizes cannot be calculated, and no conclusions concerning La and Ba effects on ruthenium dispersion can be drawn. For LaRu/C catalysts, the amount of

CO adsorbed was about 40% lower than for Ru/C, and it further decreased upon barium introduction. The observed effect can be a consequence of several effects. One of the possible reasons is a change in the ruthenium dispersion. Structural changes may cause a decrease in the amount of CO adsorption sites. However, microscopic data reported in [29] for La-Ru/C catalysts rather eliminate the possibility of lowering ruthenium dispersion upon lanthanum addition. On the contrary, lanthanum, which is present in all doped systems, is seen as a dispersion increasing agent, as revealed in the case of nickel-based catalysts [49]. The second reason for lowering the amount of adsorbed CO can be covering of the ruthenium surface by lanthanum/barium compounds. The effect increased with the increasing loading of additives in the catalyst. Hansen [59] reported that the morphology of the Ru crystals dispersed on different support materials stayed unchanged upon promotion with barium, while the TEM studies disclosed the covering of ruthenium surface with BaO_x species. The data chemically nearest to our catalytic systems were reported by Ni [54]. The authors showed that ruthenium particles in the La-promoted Ba-K-Ru/activated carbon catalyst had a relatively uniform size, and their surface might be partially covered by LaO_x and BaO_x [54]. As discussed in our previous work [29], the La introduction on the ruthenium surface electronically modifies the CO bonding on the active phase [60], which is responsible for the observed increase in catalytic activity.

3.3. XRPD

XRD characterization was performed for C support, Ru/C after ruthenium precursor reduction, and impregnated, but uncalcined, LaRu/C and BaLaRu/C catalysts. The experiments were performed for all studied materials, but for the clarity of the presentation, only one of the Ba-containing samples was chosen. The obtained diffraction patterns and the average ruthenium particles' sizes estimated on the basis of Ru diffraction signals (d_{Ru}) are presented in Figure 2.

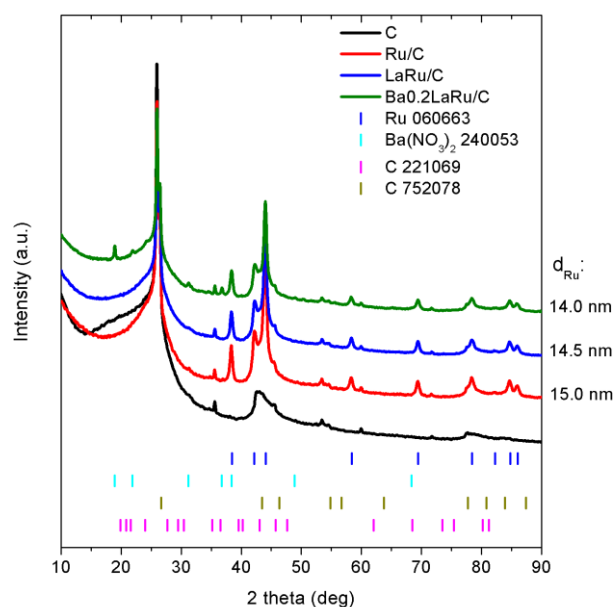


Figure 2. XRPD patterns of the of carbon support and ruthenium catalysts; d_{Ru} —the average Ru crystallite sizes in Ru/C-based systems estimated on the basis of XRPD data.

All diffraction patterns (Figure 2) contained signals corresponding to carbon (graphite). The most prominent graphite signals were visible at $2\theta = 26^\circ$ and 43° for all studied materials. The metallic ruthenium phase was visible in the prepared catalysts ($2\theta = 38^\circ$, 42° , 44° and other). The intensity of Ru signals decreased slightly upon addition of La and especially both La + Ba to Ru/C material. The effect is connected with small changes in average Ru particle sizes. The proper d_{Ru} values, estimated with use of the Scherrer

formula [57], were included in Figure 2. The value obtained for the Ru/C sample (15.0 nm) is about two times higher than that estimated on the basis of the chemisorption data (see Table 2). The possible reasons for such discrepancy was discussed in detail in our previous work [28]. Having in mind that the accuracy of the average crystallite size estimation is about 0.5 nm, it must be concluded that only a very small change in d_{Ru} was observed upon adding La/Ba + La to the Ru/C material. It was proposed that a small decrease in d_{Ru} values estimated for LaRu/C and Ba0.2LaRu/C may be connected with the partial coverage of Ru crystallites with the lanthanum/barium compounds, as discussed in Section 3.2. The interaction between external walls of crystallites with dopants adlayers can disrupt their structure [61]. In consequence, the structural ordering is present at a shorter distance, which manifests itself in lowered d_{Ru} values. There were no signals of any lanthanum-containing phase for both LaRu/C and Ba0.2LaRu/C catalysts. This means that the lanthanum that is present in the sample is well dispersed or amorphous. In the case of Ba0.2LaRu/C, signals corresponding to $\text{Ba}(\text{NO}_3)_2$ appeared, which suggests that, after catalyst preparation, some part of the barium precursor stayed in the sample in the uncalcined form.

3.4. H_2 -TPR

The TG-MS experiments, representing temperature programmed reduction, were conducted to determine whether the carbon support applied in the catalysts is resistant to undesired methanation. Additionally, we wanted to examine if the presence of two combined additives (lanthanum and barium) modifies the course of this process. It must be mentioned that the modified carbon support itself does not undergo hydrogenation to methane. Figure 3 shows the TG-MS profiles for Ru/C catalysts and three doped samples. The mass spectrometer signals corresponding to water ($m/e = 18$) and methane ($m/e = 15$) were also presented.

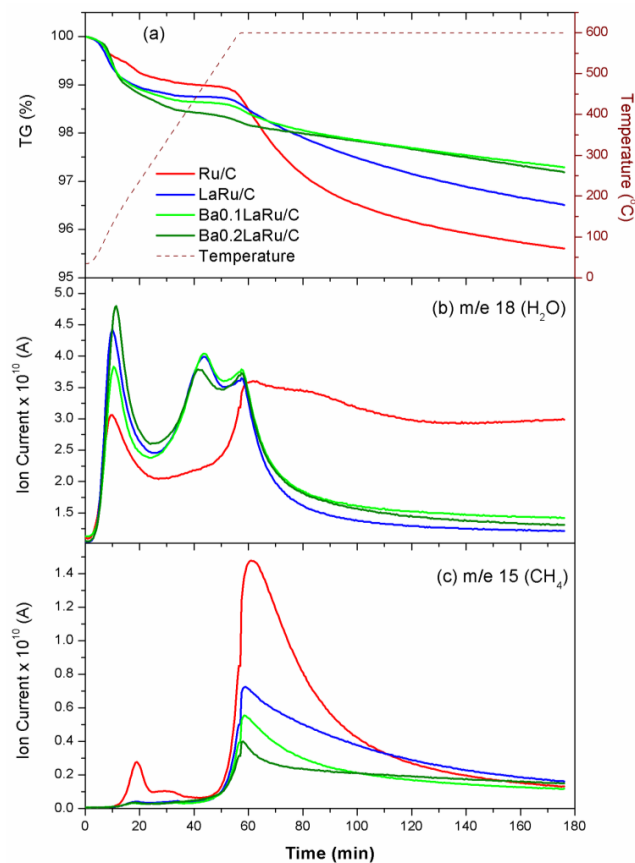


Figure 3. TG-MS profiles of the catalysts: (a) mass loss during heating to 600 °C and at the isothermal stage, (b) MS signal of water evolution, and (c) MS signal of methane evolution.

As presented in Figure 3, addition of even very low amounts of La/(La + Ba) to Ru/C catalyst changed the course of its reduction. During the experiment, generally three mass loss stages were observed (Figure 3a). The first stage of TG signal decrease (1–1.5%), which lasts until about 300 °C, is more substantial for doped samples than for the Ru/C material. This is related to the chemically richer composition of the La/(La + Ba)-doped samples. The additional, slow mass loss was observed for all materials with increasing temperature. A notable weight loss was recorded for all samples at about 550–600 °C (Figure 3a). Next, a slow decrease in TG signal was observed until the end of experiment. What should be noted is that the mass loss during the isothermal stage was the largest for the undoped Ru/C material, i.e., approx. 3%. The introduction of lanthanum decreased this value to 2%. Moreover, the co-addition of lanthanum and barium to Ru/C material resulted in a further reduction in this effect. For Ba_{0.1}LaRu/C, the mass change during the isothermal stage reached 1.22% and, for Ba_{0.2}LaRu/C, it was 1.05%.

The mass losses described above were associated mainly with the evolution of water, as confirmed by the MS signals at $m/e = 18$ (Figure 3b). Possible sources of water at the heating segment of the experiment in the case of Ru/C material are desorption from the sample surface and also reduction in the thin layer of ruthenium oxide, obtained on the surface of ruthenium crystallites during the passivation procedure. The intensity of the MS H₂O signals recorded at about 100 °C for doped samples are larger than in the case of Ru/C catalysts (Figure 3b). The introduction of lanthanum and barium to Ru/C material also resulted in the appearance of a new water MS signal at about 470 °C. The intensities of this signal were almost the same for LaRu/C and Ba_{0.1}LaRu/C samples and slightly lower for higher barium loading in the catalyst. As mentioned before, simultaneous introduction of two elements at the preparation stage causes interaction between their compounds. The more complex course of reduction in doped catalysts could be attributed to the decomposition of lanthanum/barium precursors [62] and reduction in nitrates to metal oxides [63]. It is also possible that compounds containing both La and Ba are present in the sample, similar to what was described in [64], where barium and cerium interaction resulted in the formation of barium cerate (BaCeO₃). Because of very low amounts of the added salts, no such phases could be identified through XRD studies. Therefore, it is hard to indicate whether any bimetallic La-Ba compounds are present in the catalysts. The last MS H₂O signal was recorded for all samples at the beginning of the isothermal stage. We suppose that it is possibly connected with the reduction in the oxygen-containing groups present on the carbon support surface with hydrogen, activated on reduced ruthenium particles [65,66]. For the Ru/C sample, the evolution of water was continued until the end of the experiment. In the case of the three doped samples, the intensity of these H₂O signals was comparable, regardless of the sample composition, but it rapidly decreased with time. This means that the presence of lanthanum and barium on the surface of ruthenium catalysts affects the possibility of the hydrogenation impact of Ru on adjacent surfaces.

The next interesting influence of lanthanum and barium addition to Ru/C materials is connected with methane production (Figure 3c). The source of carbon for CH₄ evolution in these systems is the support material. The carbon support can react with hydrogen in the presence of metallic ruthenium [34,67]. It is an undesired effect that the support undergoes methanation during operation in the hydrogen stream. It should be noted that the intensity of MS $m/e = 15$ signals are much lower than those connected with water. Thus, it can be concluded that methane formation occurs to a minor extent under these conditions. However, small amounts of methane ($m/e = 15$, Figure 3c) were observed for the Ru/C sample at about 200 °C. That effect was significantly reduced for lanthanum and barium-doped materials. The increased intensity of CH₄ evolution was recorded at temperatures higher than 500 °C. It was revealed that the addition of lanthanum significantly lowers the amount of evolved methane [29]. The addition of barium further enhances this positive effect, in agreement with the earlier literature reports for Ba-Ru/C catalysts [40–43]. The achieved, positive result shows that both metals used in the catalytic system act as methanation

inhibitors, despite of the chemical forms of lanthanum and barium in the doubly doped systems and that there is a possible interaction between their compounds.

3.5. Raman Spectral Analysis

The Ru/C-based samples, and also the carbon support, were examined by Raman spectroscopy before and after reduction with hydrogen. In the typical Raman spectra of carbon materials, we observe the most prominent peak, G (around 1580–1600 cm^{-1}) [34], which is assigned to a double degenerate phonon in Brillouin's zone center with E_{2g} symmetry. The G peak is associated with bond stretching of all pairs of sp^2 atoms in rings and chains. Its full width at half maximum is inversely proportional to the lifetime of the phonon and increases with the increasing concentration of defects in the material structure. Different types of defects can be defined as edges, grain boundaries, vacancies, additional atoms, and defects associated with a change in carbon hybridization (sp^2/sp^3 ratio). Peak D (around 1350 cm^{-1}) and G^* (around 1650 cm^{-1}) are activated, respectively, by a single phonon intervalley and intravalley processes, but with the presence of defects [34,68]. Peak 2D (around 2600 cm^{-1}) is due to two phonons near the K point of Brillouin zone with A'_1 symmetry. The 2D peak can consist of many components with different shapes, positions, and intensities, which depend on splitting of electronic and phonons bands [69–71]. Samples presented in Figure 4 can be classified as carbon materials with a mixture of sp^2 and sp^3 bonding. Raman spectra of these materials is dominated by the sp^2 states because visible photons prefer to excite π states. Even for highly sp^3 amorphous carbon samples, the visible Raman spectra are due to sp^2 vibrations. Thus, we can observe fundamental changes in catalysts' sp^2 structure and only indirectly changes in sp^3 structure [68].

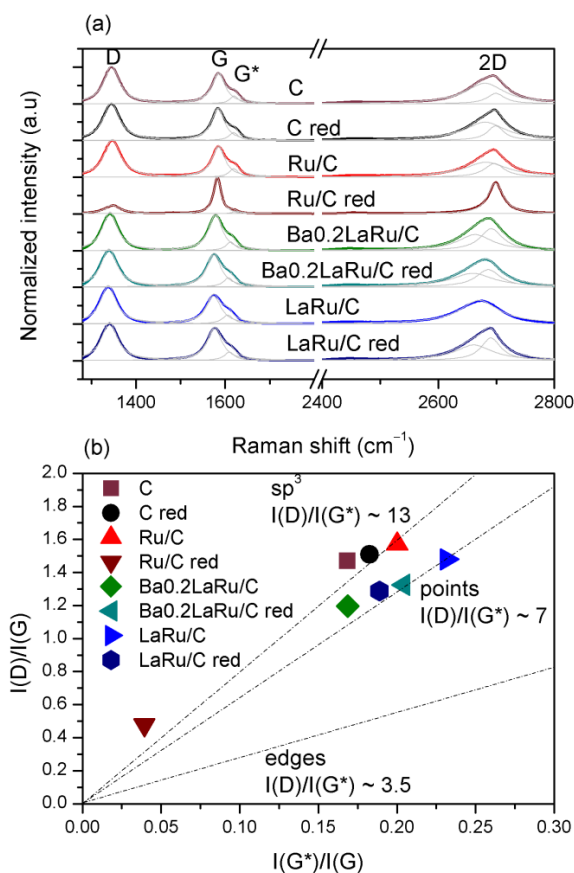


Figure 4. Raman spectroscopy of carbon supported materials: (a) Raman spectra of carbon support and studied catalysts with outlined D, G, G^* , and 2D peaks; (b) diagram of $I(G^*)/I(G)$ versus $I(D)/I(G)$, showing defect type in sp^2 structure of carbon-based samples.

It was shown (Figure 4a) that the addition of metal salts to partially graphitized carbon, the different preparation steps, and the additional reduction process, which simulates the activation of the catalyst prior to the catalytic tests, affects the Raman spectrum to a varying degree. Raman spectra of the original carbon support (C and C red, Figure 4a) differ by intensities, positions, and shapes of D, G, G*, and 2D bands, which indicate changes that are taking place in the structure of the carbon material subjected to reduction in hydrogen. For all studied catalysts, the structural defects in the carbon material are also present. However, changes in the chemical composition of materials are connected with slight differences in the obtained spectra. Ruthenium catalyst subjected to reduction (Ru/C red) stands out from the rest of the catalysts. Both G and 2D peaks were significantly narrower after reduction, which can be attributed to a decrease in the number of interlayer defects [34]. To discuss the structural differences between the samples, I(D)/I(G) intensity ratios are commonly used [72,73]. It was reported that the increase in I(D)/I(G) ratio is connected with an increase in the structural carbon disorder [74].

Intensity ratios of D and G peaks for the initial and reduced samples were estimated on the basis of Raman spectra and plotted in Figure 4b as a function of an I(G*)/I(G) intensity ratio. Dashed lines in Figure 4b present defect type in sp² structure [75]. For almost all the tested samples, the ID/IG ratio exceeds 1, which is characteristic for disordered carbon structures [73]. Most of samples are between the region of sp³ defects and point defects (vacancies), except Ru/C red, whose Raman spectrum is significantly different. The I(D)/I(G) ratio of Ru/C red is much lower than that of the other samples, which means that, in this case, the graphitic phase (sp²) significantly outweighs the sp³ phase. Additionally, the G* peak for Ru/C red has very low intensity, so most of the defects in the structure can be associated with the rest of the sp³ phase. Interestingly, for Ru/C and LaRu/C materials, we observed a decrease in the I(D)/I(G) ratio as a consequence of reduction. In the first case, the change was impressive: from 1.57 for Ru/C to 0.48 for Ru/C red. In the latter, the I(D)/I(G) ratio decreased from 1.48 for LaRu/C to 1.29 LaRu/C red. The opposite effect was obtained for Ba_{0.2}LaRu/C catalyst, from 1.20 to 1.32 after reduction.

3.6. SEM-EDX

The backscatter images of all four samples are shown in Figure 5. While regular SEM images differentiate topography, these images show a contrast between particles with different masses. Hence, ruthenium, barium, and lanthanum appear as light spots, which contrast with the dark (carbon) background. Well organized, stick-shaped structures have been visualized as carbon supports in Figure 5a. That observation confirms the fact of partial graphitization of the support material. It can be seen that the samples, which do not contain barium, i.e., Ru/C (Figure 5a) and LaRu/C (Figure 5d), contain only small, irregularly-shaped specks, which are very bright, whereas the two others have round sphere-like particles. EDX spectra of these particles shows a pronounced increase in lanthanum and barium in them in comparison to the background, where these levels are low. The presence of barium and lanthanum in the agglomerates may indicate an interaction of barium oxide with lanthanum. The elemental maps confirm that lanthanum is distributed evenly across the surface of the sample when no barium is present (Figure 6a). In contrast, the two samples with barium and lanthanum (Figure 6b,c) show that these two elements are associated with oxygen and tend to form round particles. The SEM data support our hypothesis about interaction of lanthanum and barium when introduced simultaneously on the Ru/C surface upon preparation.

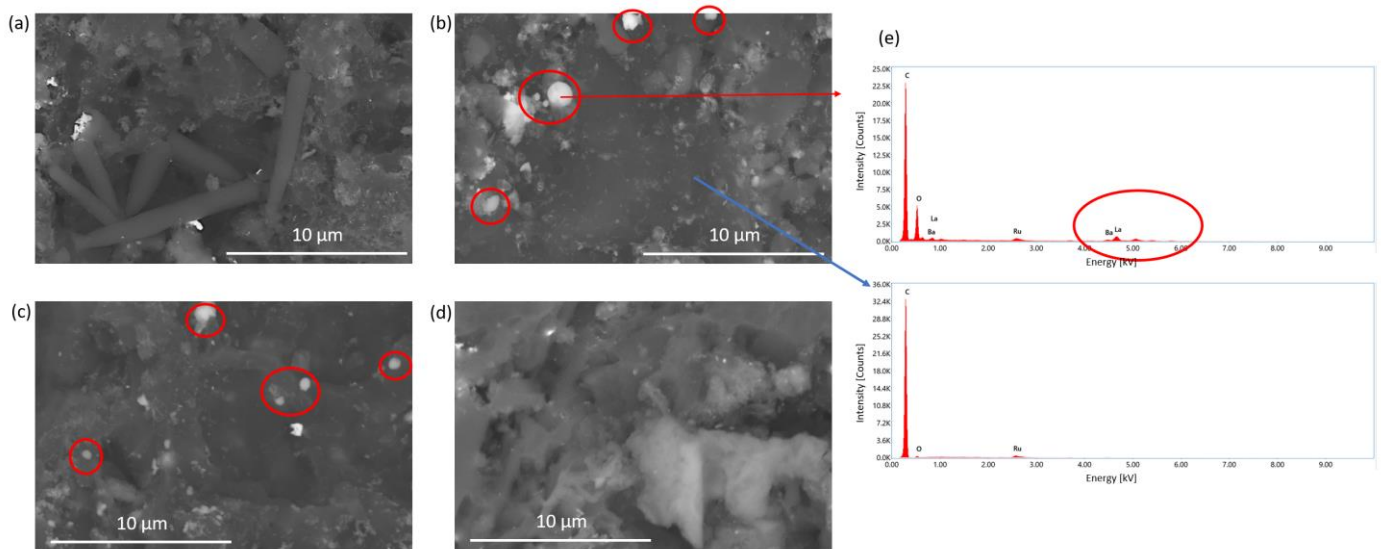


Figure 5. SEM-EDX results: backscatter images of (a) Ru/C, (b) Ba_{0.2}LaRu/C, (c) Ba_{0.1}LaRu/C and (d) LaRu/C, and (e) EDX spectra of selected points.

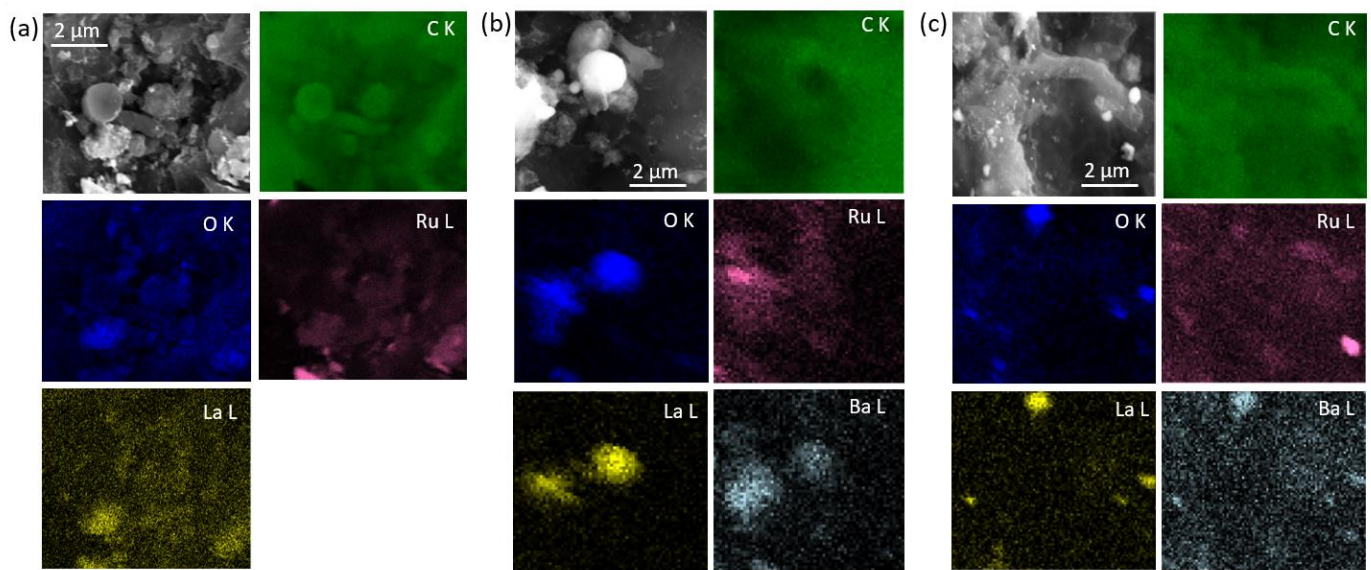


Figure 6. Elemental maps of catalysts: (a) LaRu/C, (b) Ba_{0.2}LaRu/C, and (c) Ba_{0.1}LaRu/C.

3.7. Evaluation of Catalytic Performance

The activity of all prepared samples, including the Ru/C catalyst and materials singly doped with lanthanum (LaRu/C) and doubly doped with lanthanum and barium (BaLaRu/C), was tested in a model reaction gas mixture containing 1 vol.% of CO in CO + H₂ mixture (total flow 80 cm³/min). Before activity tests, all the samples were activated in flowing hydrogen at 370 °C for 18 h. The obtained results were expressed in terms of mmol CO converted per gram of the basis material (C + Ru), per hour, and presented in Figure 7.

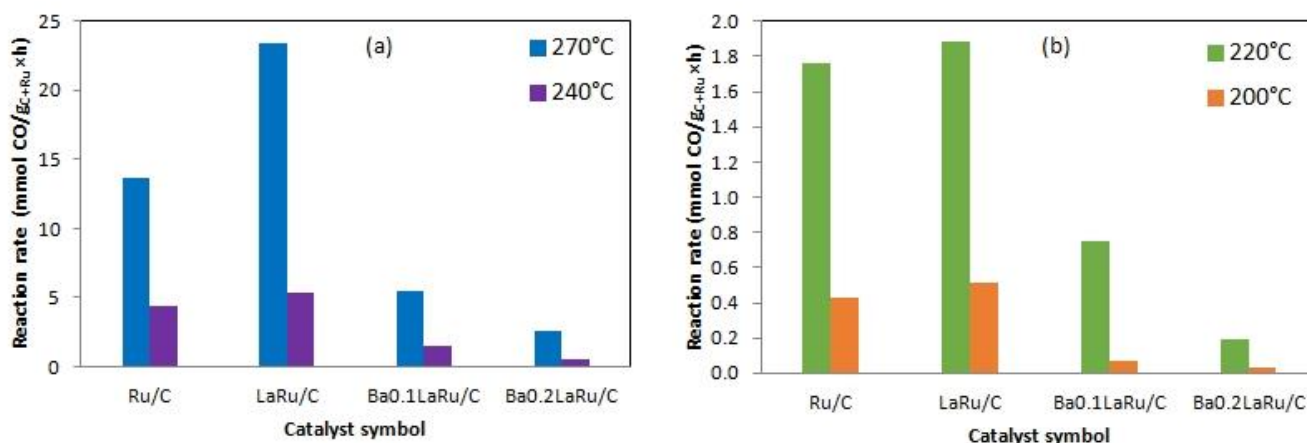


Figure 7. Catalytic activity of the Ru-based catalysts in CO hydrogenation: (a) 270 and 240 °C, (b) 220 and 200 °C.

For all tested temperatures (270, 240, 220, and 200 °C), the promoting effect of La in catalysts with only this promoter was clearly observed. The highest CO removal rate was obtained over the LaRu/C catalyst. The value of 23.46 $\text{mmol CO}/(\text{g}_{\text{C+Ru}} \times \text{h})$ reached by LaRu/C at 270 °C is almost two times higher than that obtained for the undoped Ru/C material: 13.68 $\text{mmol CO}/(\text{g}_{\text{C+Ru}} \times \text{h})$. The promoting effect of La is considerably greater than that presented in our previous paper [29]. The reaction rates obtained over Ru/C could be compared to those reported for the catalysts supported on different oxide materials, characterized by the same Ru loading (5 wt.%), similar Ru dispersion, and amounts tested (150 mg of catalyst), described in [76]. At 200 °C, the Ru/C catalyst reached 0.66 $\text{mmol CO}/(\text{g}_{\text{C+Ru}} \times \text{h})$. This activity level is lower than that obtained for Ru/CeO₂ at 215 °C: 1.98 $\text{mmol CO}/(\text{g} \times \text{h})$. However, it is higher than that obtained for Ru/SiO₂ at 215 °C: 0.47 $\text{mmol CO}/(\text{g} \times \text{h})$ [76]. However, the differences in experimental conditions, such as gas composition and the total flow rate, hinder the direct comparison.

The co-addition of lanthanum and barium to the Ru/C system caused a drastic decrease in activity by about 80% of that obtained for LaRu/C. Ba0.1LaRu/C exhibited a reaction rate even below the level for the unpromoted Ru/C material, independently of the temperature. Higher loading of barium in the sample (Ba0.2LaRu/C) caused further decrease in the amount of converted CO per ($\text{g}_{\text{C+Ru}} \times \text{h}$). The reaction rate for this sample is only about 18% of the value obtained for the Ru/C catalyst. The change in the reaction temperature does not influence the observed trend. The results indicate that lanthanum plays a promoting role in the studied system, in agreement with the literature reports [29,52], in contrast to barium. It is hard to assign the observed catalytic behaviour to the differences in the textural properties of the four catalysts, which were rather insignificant (see Table 1). However, the CO chemisorption data (Table 2) and SEM studies (Figures 5 and 6) support our hypothesis that the promoting influence of lanthanum is lost in the doubly doped catalysts, probably due to interaction between La and Ba precursors. Moreover, Raman data bring new insights into the relationship between a system's structure and its catalytic activity. The correlation between the data presented in Figure 4b with the activity levels shown in Figure 7 leads to the general conclusion that higher activity in CO hydrogenation was observed for samples for which activation in hydrogen led to a decrease in I(D)/I(G) ratio.

It is commonly known that graphite and graphene exhibit great electron conductivity [77,78]. Nitrogen-doped graphene tubes were successfully applied as the supports for a Cr–Ni₃FeN active phase by Zhou [79]. The excellent electrical conductivity of such support improved the electron transport and mass transfer in the final catalyst, thus causing outstanding electrocatalytic properties of the material [79]. Li [80] showed, for Ru/carbon catalysts for ammonia decomposition, that the more ordered graphitic structure of carbon support made electron transfer easier between the support and the ruthenium particles, which finally resulted in better catalytic activity. On the other hand, Tada [52] reported that

increased electron density in TiO₂-supported Ru particles was responsible for their high CO methanation activity. Therefore, we suggest that structural ordering of carbon support, improved during reduction in the Ru/C and LaRu/C catalysts, may be one of the factors responsible for their good methanation activity.

It must be emphasized that oxygen-containing compounds (CO and CO₂) should be eliminated from the hydrogen stream for use in fuel cells, for example. The desired product of the reaction is methane. However, carbon dioxide and C₂ hydrocarbons were also detected. The selectivity towards different products of CO hydrogenation is depicted in Figure 8 (for 270 °C) and Figure S1 (240–220–200 °C).

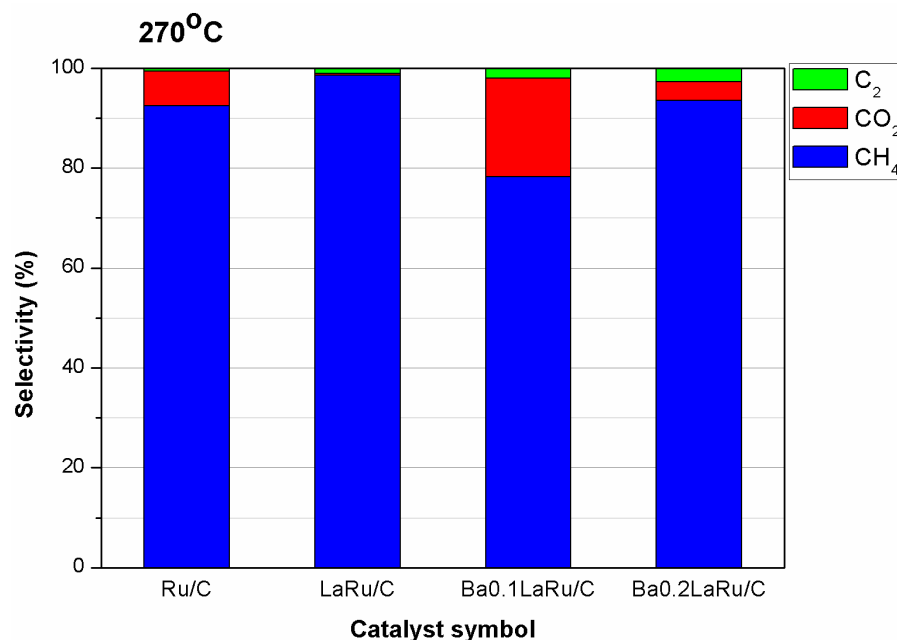


Figure 8. Selectivity towards different compounds at 270 °C observed in the course of CO hydrogenation over Ru-based catalysts.

Figure 8 reveals that the selectivity in the studied reaction depends on the catalyst composition. In the mixture of carbon-containing products analyzed at 270 °C, the highest fraction is that of methane. It is around 92% for Ru/C, above 98% for LaRu/C, and 93% for Ba0.2LaRu/C. The value obtained for the sample Ba0.1LaRu/C was the lowest, reaching only 78% (Figure 8). At other studied temperatures, the highest selectivity to methane was obtained for the LaRu/C catalyst (Figure S1), and that regularity remained unchanged within the studied temperature range. For all the catalysts, we observed an increase in the carbon dioxide ratio in the product mixture with decreasing reaction temperature. The effect was the most significant in the case of the Ba0.1LaRu/C system. CO₂ can be produced in the exothermic water–gas shift (WGS) reaction ($\text{CO} + \text{H}_2\text{O} \leftrightarrow \text{CO}_2 + \text{H}_2$; $\Delta H^\circ = -41.2 \text{ kJ/mol}$) [81]. Another possible source of CO₂ observed at temperatures below 300 °C [11] may be the Boudouard reaction: $2\text{CO} \leftrightarrow \text{C} + \text{CO}_2$ $\Delta H^\circ = -172.4 \text{ kJ/mol}$ [82]. Higher hydrocarbons (C₂) are products of Fischer-Tropsch synthesis [22], which can take place in the studied gas mixture. Our results are in agreement with the report of Zamani [55], in which the simultaneous introduction of Ba and La promoters to an iron catalyst significantly improved its WGS activity. The authors claim that the reason for this was the synergistic effect and basicity of the promoters [55]. In our case, these two elements used together also seem to promote the side reaction to methane formation (Figure S1). Comparing the selectivity results (Figure 8 and Figure S1) with those of activity (Figure 7), it should be noticed that the highest activity in CO conversion obtained in the case of the LaRu/C catalyst corresponds to a higher selectivity to methane.

To investigate the catalytic stability of the studied, doped systems, additional time on stream tests is crucial. The respective data for very similar LaRu/C catalyst can be found in [29] (Supplementary Materials). The reaction rate results obtained for the Ba_{0.1}LaRu/C catalyst are shown in Figure S2. After the initial activity drop, observed after 24 h of overheating at 300 °C in the CO + H₂ mixture, the stable activity level was observed for the next 72 h of time on stream.

The catalysts after activity tests have been additionally imaged by SEM to determine if the surface exhibits signs of carbon deposition, which could block a part of the active sites by physically covering them and, hence, contribute to loss in their activity. The results of the topography and respective backscatter images clearly show the presence of such deposits (Figure S3). The top four images (Figure S3a,b,d,e) pertain to standard activity tests, whereas the bottom two (Figure S3c,f) are those of a catalyst after time-on-stream measurements. When the deposit is large enough, its presence is evidenced by a black patch on the backscatter image (Figure S3e,f), which covers the bright spots that correspond to heavier particles, i.e., Ru, La, and Ba. When comparing Ba_{0.2}LaRu/C and LaRu/C, it can be observed that the deposits are larger in the case of the latter, more active system. It is noteworthy that the catalyst after time-on-stream tests (Ba_{0.1}LaRu/C) does not differ substantially in terms of the size of carbon deposits from the active system after standard activity tests. This may account for the initial activity loss followed by stable activity of this system in the time-on-stream experiment.

4. Conclusions

The influence of lanthanum and barium addition to Ru/C material on the textural and structural properties, as well as catalytic behavior in CO hydrogenation, have been investigated. The most favorable catalytic performance was achieved with the LaRu/C catalyst. The activity level for lanthanum + barium-doped catalysts was lower than that of the undoped Ru/C material. The introduction of lanthanum, or lanthanum and barium together, resulted in a decrease in the BET surface area and pore volume. It was revealed that both dopants successfully inhibit the undesired reaction of carbon support methanation under hydrogenation conditions. The presence of La and Ba in catalytic material substantially affected the amounts of chemisorbed CO through the Ru surface, covering or changing the nature of the Ru active sites. It was revealed that, in the doubly doped systems, an interaction between La and Ba occurs, which results in loss of promotional influence of La on Ru. We have also shown that the chemical composition and the way of material treatment change the degree of structure ordering in the carbon material. These are supposed to influence the final activity of the catalyst through charge transfer modification. These findings emphasize the essential role of understanding the state and role of different additives in designing highly active, resistant catalysts for hydrogen purification.

Supplementary Materials: The following supporting information can be downloaded at: <https://www.mdpi.com/article/10.3390/hydrogen4020027/s1>, Selectivity towards methane, carbon dioxide and C₂ hydrocarbons for CO hydrogenation over the Ru- based catalysts at 240–220 and 200 °C. Experimental conditions: mass of catalyst: 0.02 g(C + Ru); gas composition: 1 vol.% CO, 99 vol.% H₂; total flow rate: 80 cm³/min.

Author Contributions: Conceptualization, E.T.; Data curation, E.T., E.M.I. and M.O.; Formal analysis, E.T., E.M.I., M.O. and A.O.; Funding acquisition, E.T.; Investigation, E.T., A.B., E.M.I., M.O. and A.O.; Methodology, E.T., A.B., E.M.I., M.O. and A.O.; Project administration, E.T.; Resources, E.T.; Supervision, E.T.; Validation, E.T., E.M.I. and M.O.; Visualization, E.T., E.M.I. and M.O.; Writing—original draft, E.T., E.M.I. and M.O.; Writing—review and editing, E.T., E.M.I. and M.O. All authors have read and agreed to the published version of the manuscript.

Funding: This research received no external funding.

Data Availability Statement: All data are available within the paper and Supplementary Materials.

Conflicts of Interest: The authors declare no conflict of interest.

References

1. Megia, P.J.; Vizcaino, A.J.; Calles, J.A.; Carrero, A. Hydrogen Production Technologies: From Fossil Fuels toward Renewable Sources. A Mini Review. *Energy Fuels* **2021**, *35*, 16403–16415. [\[CrossRef\]](#)
2. Sharma, S.; Agarwal, S.; Jain, A. Significance of Hydrogen as Economic and Environmentally Friendly Fuel. *Energies* **2021**, *14*, 7389. [\[CrossRef\]](#)
3. Rangel, M.D.C.; Querino, P.S.; Borges, S.M.S.; Marchetti, S.G.; Assaf, J.M.; Vásquez, D.P.R.; Rodella, C.B.; Silva, T.D.F.; da Silva, A.H.M.; Ramon, A.P. Hydrogen purification over lanthanum-doped iron oxides by WGS. *Catal. Today* **2017**, *296*, 262–271. [\[CrossRef\]](#)
4. Mueller-Langer, F.; Tzimas, E.; Kaltschmitt, M.; Peteves, S. Techno-economic assessment of hydrogen production processes for the hydrogen economy for the short and medium term. *Int. J. Hydrogen Energy* **2007**, *32*, 3797–3810. [\[CrossRef\]](#)
5. Dincer, I.; Acar, C. Smart energy solutions with hydrogen options. *Int. J. Hydrogen Energy* **2018**, *43*, 8579–8599. [\[CrossRef\]](#)
6. Fiorio, J.L.; Gothe, M.L.; Kohlrausch, E.C.; Zardo, M.L.; Tanaka, A.A.; de Lima, R.B.; da Silva, A.G.M.; Garcia, M.A.S.; Vidinha, P.; Machado, G. Nanoengineering of Catalysts for Enhanced Hydrogen Production. *Hydrogen* **2022**, *3*, 218–254. [\[CrossRef\]](#)
7. IEA. *Technology Roadmap—Energy and GHG Reductions in the Chemical Industry via Catalytic Processes*; IEA: Paris, France, 2013.
8. Rosen, M.A.; Koochi-Fayegh, S. The prospects for hydrogen as an energy carrier: An overview of hydrogen energy and hydrogen energy systems. *Energy Ecol. Env.* **2016**, *1*, 10–29. [\[CrossRef\]](#)
9. Wang, Z.; Dong, C.; Tang, X.; Qin, X.; Liu, X.; Peng, M.; Xu, Y.; Song, C.; Zhang, J.; Liang, X.; et al. CO-tolerant RuNi/TiO₂ catalyst for the storage and purification of crude hydrogen. *Nat. Commun.* **2022**, *13*, 1–9. [\[CrossRef\]](#)
10. Lang, S.M.; Bernhardt, T.M.; Krstić, M.; Bonačić-Koutecký, V. The origin of the selectivity and activity of ruthenium-cluster catalysts for fuel-cell feed-gas purification: A gas-phase approach. *Angew. Chem. Int. Ed.* **2014**, *53*, 5467–5471. [\[CrossRef\]](#)
11. Panagiotopoulou, P.; Kondarides, D.I.; Verykios, X.E. Mechanistic study of the selective methanation of CO over Ru/TiO₂ catalyst: Identification of active surface species and reaction pathways. *J. Phys. Chem. C* **2011**, *115*, 1220–1230. [\[CrossRef\]](#)
12. de Cássia Colman, R.; Torres, L.A.; de Lima, A.F.F.; Appel, L.G. Removing CO and acetaldehyde from hydrogen streams generated by ethanol reforming. *Int. J. Hydrogen Energy* **2009**, *34*, 9832–9837. [\[CrossRef\]](#)
13. Kustov, A.L.; Frey, A.M.; Larsen, K.E.; Johannessen, T.; Nørskov, J.K.; Christensen, C.H. CO methanation over supported bimetallic Ni-Fe catalysts: From computational studies towards catalyst optimization. *Appl. Catal. A Gen.* **2007**, *320*, 98–104. [\[CrossRef\]](#)
14. Gao, Z.; Dai, Q.; Ma, H.; Li, Z. Ceria supported nickel catalysts for CO removal from H₂-rich gas. *J. Rare Earths* **2016**, *34*, 1213–1220. [\[CrossRef\]](#)
15. Chen, A.; Miyao, T.; Higashiyama, K.; Yamashita, H.; Watanabe, M. High catalytic performance of ruthenium-doped mesoporous nickel-aluminum oxides for selective CO methanation. *Angew. Chem. Int. Ed.* **2010**, *49*, 9895–9898. [\[CrossRef\]](#)
16. Prins, R.; Wang, A.; Xiang, L. *Introduction to Heterogeneous Catalysis*; Imperial College Press and World Scientific Publishing: London, UK; Singapore, 2016. [\[CrossRef\]](#)
17. Rönsch, S.; Schneider, J.; Matthischke, S.; Schlüter, M.; Götz, M.; Lefebvre, J.; Prabhakaran, P.; Bajohr, S. Review on methanation – From fundamentals to current projects. *Fuel* **2016**, *166*, 276–296. [\[CrossRef\]](#)
18. Panagiotopoulou, P. Hydrogenation of CO₂ over supported noble metal catalysts. *Appl. Catal. A Gen.* **2017**, *542*, 63–70. [\[CrossRef\]](#)
19. Cant, N.W.; Bell, A.T. Studies of carbon monoxide hydrogenation over ruthenium using transient response techniques. *J. Catal.* **1982**, *73*, 257–271. [\[CrossRef\]](#)
20. Dagle, R.A.; Wang, Y.; Xia, G.G.; Strohm, J.J.; Holladay, J.; Palo, D.R. Selective CO methanation catalysts for fuel processing applications. *Appl. Catal. A Gen.* **2007**, *326*, 213–218. [\[CrossRef\]](#)
21. Tada, S.; Kikuchi, R. Preparation of Ru nanoparticles on TiO₂ using selective deposition method and their application to selective CO methanation. *Catal. Sci. Technol.* **2014**, *4*, 26–29. [\[CrossRef\]](#)
22. Eckle, S.; Denkwitz, Y.; Behm, R.J. Activity, selectivity, and adsorbed reaction intermediates/reaction side products in the selective methanation of CO in reformat gases on supported Ru catalysts. *J. Catal.* **2010**, *269*, 255–268. [\[CrossRef\]](#)
23. Garbarino, G.; Bellotti, D.; Riani, P.; Magistri, L.; Busca, G. Methanation of carbon dioxide on Ru/Al₂O₃ and Ni/Al₂O₃ catalysts at atmospheric pressure: Catalysts activation, behaviour and stability. *Int. J. Hydrogen Energy* **2015**, *40*, 9171–9182. [\[CrossRef\]](#)
24. Cisneros, S.; Chen, S.; Diemant, T.; Bansmann, J.; Abdel-Mageed, A.M.; Goepel, M.; Olesen, S.E.; Welter, E.S.; Parlinska-Wojtan, M.; Gläser, R.; et al. Effects of SiO₂-doping on high-surface-area Ru/TiO₂ catalysts for the selective CO methanation. *Appl. Catal. B Environ.* **2021**, *282*, 119483. [\[CrossRef\]](#)
25. Chen, S.; Abdel-Mageed, A.M.; Gauckler, C.; Olesen, S.E.; Chorkendorff, I.; Behm, R.J. Selective CO methanation on isostructural Ru nanocatalysts: The role of support effects. *J. Catal.* **2019**, *373*, 103–115. [\[CrossRef\]](#)
26. Tada, S.; Kikuchi, R.; Urasaki, K.; Satokawa, S. Effect of reduction pretreatment and support materials on selective CO methanation over supported Ru catalysts. *Appl. Catal. A Gen.* **2011**, *404*, 149–154. [\[CrossRef\]](#)
27. Eckle, S.; Anfang, H.G.; Behm, R.J. What drives the selectivity for CO methanation in the methanation of CO₂-rich reformat gases on supported Ru catalysts? *Appl. Catal. A Gen.* **2011**, *391*, 325–333. [\[CrossRef\]](#)
28. Truszkiewicz, E.; Zegadło, K.; Wojda, D.; Mierzwa, B.; Kepiński, L. The effect of the ruthenium crystallite size on the activity of Ru/carbon systems in CO methanation. *Top. Catal.* **2017**, *60*, 1299–1305. [\[CrossRef\]](#)

29. Truskiewicz, E.; Bielecka, A.; Moszyński, D.; Ostrowski, A. Lowering risk of methanation of carbon support in Ru/carbon catalysts for CO methanation by adding lanthanum. *Int. J. Hydrogen Energy* **2023**. [[CrossRef](#)]
30. Méndez-Mateos, D.; Barrio, V.L.; Requies, J.M.; Cambra, J.F. Effect of the addition of alkaline earth and lanthanide metals for the modification of the alumina support in Ni and Ru catalysts in CO₂ methanation. *Catalysts* **2021**, *11*, 353. [[CrossRef](#)]
31. Gonzalez, R.D.; Miura, H. Methanation and Fischer-Tropsch studies on potassium-promoted silica-supported Ru catalysts. *J. Catal.* **1982**, *77*, 338–347. [[CrossRef](#)]
32. Petala, A.; Panagiotopoulou, P. Methanation of CO₂ over alkali-promoted Ru/TiO₂ catalysts: I. Effect of alkali additives on catalytic activity and selectivity. *Appl. Catal. B Environ.* **2018**, *224*, 919–927. [[CrossRef](#)]
33. Sakakini, B.H. Temperature-programmed surface reaction (TPSR) of pre-adsorbed carbon CO and COH₂ synthesis over Ru-CsAl₂O₃ catalysts. *J. Mol. Catal. A Chem.* **1997**, *127*, 203–209. [[CrossRef](#)]
34. Iost, K.N.; Borisov, V.A.; Temerev, V.L.; Smirnova, N.S.; Surovikin, Y.V.; Trenikhin, M.V.; Arbuzov, A.B.; Gulyaeva, T.I.; Shlyapin, D.A.; Tsyrlunikov, P.G.; et al. Effect of the carbon support graphitization on the activity and thermal stability of Ru-Ba-Cs/C ammonia decomposition catalysts. *React. Kinet. Mech. Catal.* **2019**, *127*, 85–102. [[CrossRef](#)]
35. Xiong, J.; Dong, X.; Li, L. CO selective methanation in hydrogen-rich gas mixtures over carbon nanotube supported Ru-based catalysts. *J. Nat. Gas Chem.* **2012**, *21*, 445–451. [[CrossRef](#)]
36. Xiong, J.; Dong, X.; Song, Y.; Dong, Y. A high performance Ru-ZrO₂/carbon nanotubes-Ni foam composite catalyst for selective CO methanation. *J. Power Sources* **2013**, *242*, 132–136. [[CrossRef](#)]
37. Jiménez, V.; Panagiotopoulou, P.; Sánchez, P.; Valverde, J.L.; Romero, A. Synthesis and characterization of ruthenium supported on carbon nanofibers with different graphitic plane arrangements. *Chem. Eng. J.* **2011**, *168*, 947–954. [[CrossRef](#)]
38. Kumi, D.O.; Dlamini, M.W.; Phaahlamohlaka, T.N.; Mhlanga, S.D.; Coville, N.J.; Scurrrell, M.S. Selective CO Methanation Over Ru Supported on Carbon Spheres: The Effect of Carbon Functionalization on the Reverse Water Gas Shift Reaction. *Catal. Lett.* **2018**, *148*, 3502–3513. [[CrossRef](#)]
39. Truskiewicz, E.; Kowalczyk, K.; Dębska, A.; Wojda, D.; Iwanek, E.; Kępiński, L.; Mierzwa, B. Methanation of CO on Ru/graphitized-carbon catalysts: Effects of the preparation method and the carbon support structure. *Int. J. Hydrogen Energy* **2020**, *45*, 31985–31999. [[CrossRef](#)]
40. Truskiewicz, E.; Raróg-Pilecka, W.; Zybert, M.; Wasilewska-Stefańska, M.; Topolska, E.; Michalska, K. Effect of the ruthenium loading and barium addition on the activity of ruthenium/carbon catalysts in carbon monoxide methanation. *Pol. J. Chem. Technol.* **2014**, *16*, 106–110. [[CrossRef](#)]
41. Zeng, H.S.; Hihara, T.; Inazu, K.; Aika, K.I. Effect of methanation of active carbon support on the barium-promoted ruthenium catalyst for ammonia synthesis. *Catal. Lett.* **2001**, *76*, 193–199. [[CrossRef](#)]
42. Kowalczyk, Z.; Jodzis, S.; Raróg, W.; Zieliński, J.; Pielaszek, J. Effect of potassium and barium on the stability of a carbon-supported ruthenium catalyst for the synthesis of ammonia. *Appl. Catal. A Gen.* **1998**, *173*, 153–160. [[CrossRef](#)]
43. Rossetti, I.; Pernicone, N.; Forni, L. Promoters effect in Ru/C ammonia synthesis catalyst. *Appl. Catal. A Gen.* **2001**, *208*, 271–278. [[CrossRef](#)]
44. AlKetbi, M.; Polychronopoulou, K.; Abi Jaoude, M.; Vasiliades, M.A.; Sebastian, V.; Hinder, S.J.; Baker, M.A.; Zedan, A.F.; Efstathiou, A.M. Cu-Ce-La-Ox as efficient CO oxidation catalysts: Effect of Cu content. *Appl. Surf. Sci.* **2020**, *505*, 144474. [[CrossRef](#)]
45. Ahmad, W.; Younis, M.N.; Shawabkeh, R.; Ahmed, S. Synthesis of lanthanide series (La, Ce, Pr, Eu & Gd) promoted Ni/γ-Al₂O₃ catalysts for methanation of CO₂ at low temperature under atmospheric pressure. *Catal. Commun.* **2017**, *100*, 121–126. [[CrossRef](#)]
46. Siakavelas, G.; Charisiou, N.; AlKhoori, A.; Sebastian, V.; Hinder, S.; Baker, M.; Yentekakis, I.; Polychronopoulou, K.; Goula, M. Highly selective and stable Ni/La-M (M=Sm, Pr, and Mg)-CeO₂ catalysts for CO₂ methanation. *J. CO₂ Util.* **2021**, *51*, 101618. [[CrossRef](#)]
47. Song, M.; Shi, L.; Xu, X.; Du, X.; Chen, Y.; Zhuang, W.; Tao, X.; Sun, L.; Xu, Y. Ni/M/SiO₂ catalyst (M=La, Ce or Mg) for CO₂ methanation: Importance of the Ni active sites. *J. CO₂ Util.* **2022**, *64*. [[CrossRef](#)]
48. Siakavelas, G.; Charisiou, N.; AlKhoori, S.; AlKhoori, A.; Sebastian, V.; Hinder, S.; Baker, M.; Yentekakis, I.; Polychronopoulou, K.; Goula, M. Highly selective and stable nickel catalysts supported on ceria promoted with Sm₂O₃, Pr₂O₃ and MgO for the CO₂ methanation reaction. *Appl. Catal. B Environ.* **2020**, *282*, 119562. [[CrossRef](#)]
49. Quindimil, A.; De-La-Torre, U.; Pereda-Ayo, B.; González-Marcos, J.A.; González-Velasco, J.R. Ni catalysts with La as promoter supported over Y- and BETA- zeolites for CO₂ methanation. *Appl. Catal. B Environ.* **2018**, *238*, 393–403. [[CrossRef](#)]
50. Zhang, T.; Liu, Q. Lanthanum-Modified MCF-Derived Nickel Phyllosilicate Catalyst for Enhanced CO₂ Methanation: A Comprehensive Study. *ACS Appl. Mater. Interfaces* **2020**, *12*, 19587–19600. [[CrossRef](#)]
51. Wierzbicki, D.; Motak, M.; Grzybek, T.; Gálvez, M.E.; Da Costa, P. The influence of lanthanum incorporation method on the performance of nickel-containing hydrotalcite-derived catalysts in CO₂ methanation reaction. *Catal. Today* **2018**, *307*, 205–211. [[CrossRef](#)]
52. Tada, S.; Kikuchi, R.; Takagaki, A.; Sugawara, T.; Oyama, S.T.; Satokawa, S. Effect of metal addition to Ru/TiO₂ catalyst on selective CO methanation. *Catal. Today* **2014**, *232*, 16–21. [[CrossRef](#)]

53. Tada, S.; Kikuchi, R. Mechanistic study and catalyst development for selective carbon monoxide methanation. *Catal. Sci. Technol.* **2015**, *5*, 3061–3070. [[CrossRef](#)]
54. Ni, J.; Lin, J.; Wang, X.; Lin, B.; Lin, J.; Jiang, L. Promoting Effects of Lanthan on Ru/AC for Ammonia Synthesis: Tuning Catalytic Efficiency and Stability Simultaneously. *Chemistryselect* **2017**, *2*, 6040–6046. [[CrossRef](#)]
55. Zamani, Y.; Bakavoli, M.; Rahimizadeh, M.; Mohajeri, A.; Seyedi, S.M. Synergetic Effect of La and Ba Promoters on Nanostructured Iron Catalyst in Fischer-Tropsch Synthesis. *Cuihua Xuebao/Chin. J. Catal.* **2012**, *33*, 1119–1124. [[CrossRef](#)]
56. Ronduda, H.; Zybert, M.; Patkowski, W.; Ostrowski, A.; Jodłowski, P.; Szymański, D.; Kępiński, L.; Raróg-Pilecka, W. Boosting the Catalytic Performance of Co/Mg/La Catalyst for Ammonia Synthesis by Selecting a Pre-Treatment Method. *Catalysts* **2021**, *11*, 941. [[CrossRef](#)]
57. Jiménez, V.; Sánchez, P.; Panagiotopoulou, P.; Valverde, J.L.; Romero, A. Methanation of CO, CO₂ and selective methanation of CO, in mixtures of CO and CO₂, over ruthenium carbon nanofibers catalysts. *Appl. Catal. A Gen.* **2010**, *390*, 35–44. [[CrossRef](#)]
58. Borodziński, A.; Bonarowska, M. Relation between Crystallite Size and Dispersion on Supported Metal Catalysts. *Langmuir* **1997**, *13*, 5613–5620. [[CrossRef](#)]
59. Hansen, T.W.; Hansen, P.L.; Dahl, S.; Jacobsen, C.J. Support Effect and Active Sites on Promoted Ruthenium Catalysts for Ammonia Synthesis. *Catal. Lett.* **2002**, *84*, 7–12. [[CrossRef](#)]
60. Wang, L.; Zhang, T.; Wu, Y.; Ma, Q.; Gong, N.; Yang, J.; Xie, H.; Zhang, M.; Ma, J.; Tan, Y. Promotion effect of La on oxygen vacancy formation over Zn-Cr based catalyst for isobutanol synthesis from syngas. *Fuel* **2020**, *288*, 119633. [[CrossRef](#)]
61. Beck, A.; Huang, X.; Artiglia, L.; Zabilskiy, M.; Wang, X.; Rzepka, P.; Palagin, D.; Willinger, M.-G.; van Bokhoven, J.A. The dynamics of overlayer formation on catalyst nanoparticles and strong metal-support interaction. *Nat. Commun.* **2020**, *11*, 1–8. [[CrossRef](#)]
62. Zeng, H.S.; Inazu, K.; Aika, K.-I. The Working State of the Barium Promoter in Ammonia Synthesis over an Active-Carbon-Supported Ruthenium Catalyst Using Barium Nitrate as the Promoter Precursor. *J. Catal.* **2002**, *211*, 33–41. [[CrossRef](#)]
63. Bardwell, C.J.; Bickley, R.I.; Poulston, S.; Twigg, M.V. Thermal decomposition of bulk and supported barium nitrate. *Thermochim. Acta* **2015**, *613*, 94–99. [[CrossRef](#)]
64. Tarka, A.; Zybert, M.; Ronduda, H.; Patkowski, W.; Mierzwa, B.; Kępiński, L.; Raróg-Pilecka, W. On Optimal Barium Promoter Content in a Cobalt Catalyst for Ammonia Synthesis. *Catalysts* **2022**, *12*, 199. [[CrossRef](#)]
65. Guo, Y.; Mei, S.; Yuan, K.; Wang, D.-J.; Liu, H.-C.; Yan, C.-H.; Zhang, Y.-W. Low-Temperature CO₂ Methanation over CeO₂-Supported Ru Single Atoms, Nanoclusters, and Nanoparticles Competitively Tuned by Strong Metal-Support Interactions and H-Spillover Effect. *ACS Catal.* **2018**, *8*, 6203–6215. [[CrossRef](#)]
66. Qin, Y.; Bai, X. Hydrogenation of N-ethylcarbazole over Ni-Ru alloy nanoparticles loaded on graphitized carbon prepared by carbothermal reduction. *Fuel* **2021**, *307*, 121921. [[CrossRef](#)]
67. Zheng, X.; Zhang, S.; Xu, J.; Wei, K. Effect of thermal and oxidative treatments of activated carbon on its surface structure and suitability as a support for barium-promoted ruthenium in ammonia synthesis catalysts. *Carbon* **2002**, *40*, 2597–2603. [[CrossRef](#)]
68. Ferrari, A.C. Raman spectrum of graphene and graphene layers. *Solid State Commun.* **2007**, *143*, 47–57. [[CrossRef](#)]
69. Dresselhaus, M.; Jorio, A.; Saito, R. Characterizing Graphene, Graphite, and Carbon Nanotubes by Raman Spectroscopy. *Annu. Rev. Condens. Matter Phys.* **2010**, *1*, 89–108. [[CrossRef](#)]
70. Ferrari, A.C.; Basko, D.M. Raman spectroscopy as a versatile tool for studying the properties of graphene. *Nat. Nanotechnol.* **2013**, *8*, 235–246. [[CrossRef](#)]
71. Ferrari, A.C.; Meyer, J.C.; Scardaci, V.; Casiraghi, C.; Lazzeri, M.; Mauri, F.; Piscanec, S.; Jiang, D.; Novoselov, K.S.; Roth, S.; et al. Raman spectrum of graphene and graphene layers. *Phys. Rev. Lett.* **2006**, *97*, 187401. [[CrossRef](#)]
72. Lin, B.; Guo, Y.; Cao, C.; Ni, J.; Lin, J.; Jiang, L. Carbon support surface effects in the catalytic performance of Ba-promoted Ru catalyst for ammonia synthesis. *Catal. Today* **2018**, *316*, 230–236. [[CrossRef](#)]
73. Iost, K.N.; Borisov, V.A.; Temerev, V.L.; Surovikin, Y.V.; Pavluchenko, P.E.; Trenikhin, M.V.; Lupanova, A.A.; Arbuzov, A.B.; Shlyapin, D.A.; Tsyrlunikov, P.G.; et al. Study on the metal-support interaction in the Ru/C catalysts under reductive conditions. *Surfaces Interfaces* **2018**, *12*, 95–101. [[CrossRef](#)]
74. Tejada, L.M.M.; Muñoz, A.; Centeno, M.A.; Odriozola, J.A. In-situ Raman spectroscopy study of Ru/TiO₂ catalyst in the selective methanation of CO. *J. Raman Spectrosc.* **2015**, *47*, 189–197. [[CrossRef](#)]
75. Eckmann, A.; Felten, A.; Mishchenko, A.; Britnell, L.; Krupke, R.; Novoselov, K.S.; Casiraghi, C. Probing the Nature of Defects in Graphene by Raman Spectroscopy. *Nano Lett.* **2012**, *12*, 3925–3930. [[CrossRef](#)] [[PubMed](#)]
76. Panagiotopoulou, P.; Kondarides, D.I.; Verykios, X.E. Selective methanation of CO over supported Ru catalysts. *Appl. Catal. B Environ.* **2009**, *88*, 470–478. [[CrossRef](#)]
77. Zhang, X.; Han, R.; Liu, Y.; Li, H.; Shi, W.; Yan, X.; Zhao, X.; Li, Y.; Liu, B. Porous and graphitic structure optimization of biomass-based carbon materials from 0D to 3D for supercapacitors: A review. *Chem. Eng. J.* **2023**, *460*. [[CrossRef](#)]
78. Buaki-Sogó, M.; Zubizarreta, L.; García-Pellicer, M.; Quijano-López, A. Sustainable Carbon as Efficient Support for Metal-Based Nanocatalyst: Applications in Energy Harvesting and Storage. *Molecules* **2020**, *25*, 3123. [[CrossRef](#)] [[PubMed](#)]

79. Zhou, Q.; Song, G.; Zou, J.; Luo, S.; Meng, A.; Li, Z. Chromium doping and in-grown heterointerface construction for modifying Ni₃FeN toward bifunctional electrocatalyst toward alkaline water splitting. *Int. J. Hydrogen Energy* **2023**, *48*, 15921–15933. [[CrossRef](#)]
80. Li, L.; Zhu, Z.; Yan, Z.; Lu, G.; Rintoul, L. Catalytic ammonia decomposition over Ru/carbon catalysts: The importance of the structure of carbon support. *Appl. Catal. A Gen.* **2007**, *320*, 166–172. [[CrossRef](#)]
81. Muñoz-Murillo, A.; Martínez, T.L.M.; Domínguez, M.; Odriozola, J.A.; Centeno, M. Selective CO methanation with structured RuO₂/Al₂O₃ catalysts. *Appl. Catal. B Environ.* **2018**, *236*, 420–427. [[CrossRef](#)]
82. Gao, J.; Liu, Q.; Gu, F.; Liu, B.; Zhong, Z.; Su, F. Recent advances in methanation catalysts for the production of synthetic natural gas. *RSC Adv.* **2015**, *5*, 22759–22776. [[CrossRef](#)]

Disclaimer/Publisher's Note: The statements, opinions and data contained in all publications are solely those of the individual author(s) and contributor(s) and not of MDPI and/or the editor(s). MDPI and/or the editor(s) disclaim responsibility for any injury to people or property resulting from any ideas, methods, instructions or products referred to in the content.